Dalton Transactions

PAPER

View Article Online
View Journal | View Issue

Cite this: *Dalton Trans.*, 2018, **47**, 12345

Energy transfer between Eu^{3+} and Nd^{3+} in near-infrared emitting β-triketonate coordination polymers†

Laura Abad Galán,[a,b] Alexandre N. Sobolev,[c,d] Brian W. Skelton,[c] Eli Zysman-Colman, *[b] Mark I. Ogden *[a] and Massimiliano Massi *[a]

Received 19th June 2018,
Accepted 20th July 2018

DOI: 10.1039/c8dt02499e

rsc.li/dalton

Isomorphous β-triketonate-based lanthanoid polymers containing tris(4-methylbenzoyl)methanide (**mtbm**) and Rb^+ with formula $\{[Ln(Rb)(\mathbf{mtbm})_4]_2\}_n$ (Ln = Eu^{3+} and Nd^{3+}) have been synthesised and structurally characterised. The photophysical properties for the Nd^{3+} complex presented relatively long lifetimes and high quantum yields in comparison with analogous β-diketonate complexes. Mixed lanthanoid complexes were also formed and their luminescence properties studied, with effective sensitisation of the $^4F_{3/2}$ of Nd^{3+} *via* the $^5D_0$ of Eu^{3+}, which is to the best of our knowledge the first example of Eu^{3+} to Nd^{3+} sensitisation in a structurally defined coordination complex or polymer.

Introduction

Much attention has been paid to materials incorporating trivalent lanthanoid cations due to their unique photophysical properties such as their line-like emission spectra and their long-lived excited state lifetimes as a result of intraconfigurational f–f transitions. In addition, their emission colours range from the UV to the near infrared (NIR), and it is exclusively characteristic of the specific lanthanoid cation (*e.g.* red emission from europium or green emission from terbium). The NIR region is of particular interest due to potential applications in a wide range of fields including night vision devices, telecommunication signalling and life science.[1–6] Despite the listed advantages, trivalent lanthanoid cations cannot be directly excited with high efficiency, as intraconfigurational f–f transitions are parity and often spin forbidden. Therefore, π-conjugated ligands are routinely used as sensitisers, because of their greater efficiency in absorbing incident light with consequent energy transfer to lanthanoid excited states. This alternative pathway, which is termed antenna effect, is well established and is generally rationalised as energy transfer from the triplet state of the conjugated ligands, populated *via* intersystem crossing due to the strong spin–orbit coupling of the lanthanoid elements, to the excited energy levels of the lanthanoid cation.[7,8]

Furthermore, in the design of emissive lanthanoid complexes it is also necessary to avoid high energy vibrations in close proximity to the metal centre, such as the presence of OH and NH bonds. The activation of vibrational modes of these bonds acts as an efficient quencher for lanthanoid excited states. In the case of NIR emission, which is of particular interest here, CH bonds can also become an efficient source of quenching.[7]

β-Diketones with aromatic substituents, such as dibenzoylmethane, have commonly been used as antenna ligands because of their good chelating properties and their ability to effectively sensitise the trivalent lanthanoid excited states, particularly in the solid state.[9] Of the potential near-IR emitting systems, Nd^{3+} diketonate complexes have been studied in less detail than the Yb^{3+} and Er^{3+} compounds. Reported quantitative data (quantum yields, lifetimes) are very limited, despite the fact that a variety of Nd^{3+} β-diketonate complexes can be found in the literature over the last couple of decades.[10–17] As for all of the near-IR emitting systems, the design of the Nd^{3+} β-diketonate complexes typically involves two main strategies to improve photophysical properties: (i) adjusting the triplet state energy of the antenna in order to optimise energy transfer to Nd^{3+} and (ii) minimising the nonradiative relaxation pathways.[13,14]

In extending the coordination chemistry of luminescent lanthanoid β-diketonate complexes, we have been recently

[a]*School of Life and Molecular Science and Curtin Institute for Functional Molecules and Interfaces, Curtin University, Kent Street, Bentley 6102, WA, Australia. E-mail: m.massi@curtin.edu.au, m.ogden@curtin.edu.au*
[b]*Organic Semiconductor Centre, EaStCHEM School of Chemistry, University of St Andrews, St Andrews, Fife, KY16 9ST, UK. E-mail: eli.zysman-colman@st-andrews.ac.uk*
[c]*School of Molecular Sciences, M310, University of Western Australia, Perth 6009, WA, Australia*
[d]*Centre for Microscopy, Characterisation and Analysis, M310, University of the Western Australia, Perth 6009, WA, Australia*

†Electronic supplementary information (ESI) available. CCDC 1829212, 1829213, 1829214, 1829215, 1829216 and 1829217. For ESI and crystallographic data in CIF or other electronic format see DOI: 10.1039/c8dt02499e

exploring the use of β-triketonate molecules as antenna ligands for lanthanoids. These ligands have been found to support the formation of unique assemblies that display particularly enhanced ytterbium and erbium emission properties. Our previous studies with tris-benzoylmethane (**tbm**H) and tris(4-methylbenzoyl)methane (**mtbm**H) resulted in the isolation of tetranuclear assemblies and polymeric structures of formulation $[Ln(Ae{\cdot}HOEt)(\mathbf{tbm})_4]_2$ (Ln^{3+} = Eu^{3+}, Er^{3+}, Yb^{3+}/Ae^{+} = Na^{+}, K^{+}, Rb^{+})[18,19] and $\{[Ln(Cs)(\mathbf{mtbm})_4]_2\}_n$ (Ln^{3+} = Eu^{3+} and Er^{3+}),[20] respectively. In contrast, our initial attempts to isolate the corresponding neodymium analogues were not successful and their photophysical properties remained unknown.

In this work, we report the successful extension of these studies to neodymium-containing assemblies using both **tbm**H and **mtbm**H ligands in the presence of RbOH and CsOH. The syntheses, crystal structures and emission properties of the resulting assemblies are reported.

Furthermore, since the structure of these complexes were found to be similar for the different lanthanoids, we have studied the formation of mixed assemblies for the purpose of investigating energy transfer processes or multiple emission from the same material. Excited states of a lanthanoid have been previously exploited to sensitise excited states of another lanthanoid.[21–24] This approach is well established for certain pairings with NIR emitters, for example sensitisation of erbium luminescence *via* energy transfer from the $^2F_{5/2}$ excited state of trivalent ytterbium,[25–27] or ytterbium luminescence *via* visible emitters such as terbium or europium.[28,29] In contrast, to our knowledge, neodymium sensitisation *via* other lanthanoids has not been reported in coordination complexes. Only three examples have been reported where Eu/Nd energy migration was used to determine the lanthanoid–lanthanoid distance following pure Förster mechanisms.[30–32] However, these studies are focused on the quenching of the europium excited states but do not report any associated near-IR emission from the neodymium centres. This sensitisation process for neodymium emission has been seen in the case of Eu/Nd doped glasses,[33,34] so should also be possible in the comparatively well-defined structure of a coordination complex. Indeed, this study presents the first example of a coordination complex with effective lanthanoid-lanthanoid energy transfer from the $^5D_0$ of Eu^{3+} to the 4f* of Nd^{3+}, leading to dual emission.

Experimental

General procedures

All reagents and solvents were purchased from chemical suppliers and used as received without further purification. The ligand tribenzoylmethane (**tbm**H), was prepared as previously reported.[31] Hydrated $LnCl_3$ (Ln = Eu^{3+}, Er^{3+}, Yb^{3+}) was prepared by the reaction of Ln_2O_3 with hydrochloric acid (5 M), followed by evaporation of the solvent under reduced pressure. Infrared spectra (IR) were recorded on solid-state samples using an attenuated total reflectance PerkinElmer Spectrum 100 FT-IR. IR spectra were recorded from 4000 to 650 cm^{-1}; the intensities of the IR bands are reported as strong (s), medium (m), or weak (w), with broad (br) bands also specified. Melting points were determined using a BI Barnsted Electrothermal 9100 apparatus. Elemental analyses were obtained at Curtin University, Australia. Nuclear magnetic resonance (NMR) spectra were recorded using a Bruker Avance 400 spectrometer (400.1 MHz for ^1H; 100 MHz for ^{13}C) at 300 K. The data were acquired and processed by the Bruker TopSpin 3.1 software. All of the NMR spectra were calibrated to residual solvent signals.

Selected equations

The values of the radiative lifetime (τ_R), and intrinsic quantum yield (Φ_{Ln}^{Ln}), can be calculated with the following equations.[36]

$$\frac{1}{\tau_R} = 14.65\ s^{-1} \times n^3 \times \frac{I_{Tot}}{I_{MD}} \quad (1)$$

In eqn (1), the refractive index (n) of the solvent is used (assumed value of 1.5 in the solid state), the value 14.65 s^{-1} is the spontaneous emission probability of the $^7F_1 \leftarrow {}^5D_0$ transition reported previously. I_{Tot} is the total integration of the Eu^{3+} emission spectrum, and I_{MD} is the integration of the $^7F_1 \leftarrow {}^5D_0$ transition.

$$\Phi_{Ln}^{Ln} = \frac{\tau_{obs}}{\tau_R} \quad (2)$$

The sensitisation efficiency (η_{sens}) can be determined using eqn (3) below:

$$\eta_{sens} = \frac{\Phi_{Ln}^{L}}{\Phi_{Ln}^{Ln}} \quad (3)$$

The rate of energy transfer (K_{ET}) and quantum efficiency of energy transfer (Φ_{ET}) can be calculated according to the following equations:

$$k_{ET} = \frac{1}{\tau_q} - \frac{1}{\tau_u} \quad (4)$$

$$\Phi_{ET} = 1 - \frac{\tau_q}{\tau_u} \quad (5)$$

In eqn (4) and (5), τ_q and τ_u are the $^5D_0$ decay lifetime of Eu^{3+} in the presence or absence of the quencher (Nd^{3+}), respectively.

For dipole–dipole exchange mechanisms or Förster the donor–acceptor distance (R_{DA}) can be calculated following eqn (6):

$$\Phi_{FRET} = \frac{1}{1 + \left(\frac{R_{DA}}{R_0}\right)^6} \quad (6)$$

where R_0 is the critical distance for a 50% transfer, being tabulated to be 9.05 Å for the Eu^{3+}–Nd^{3+} pair.[35]

Photophysical measurements

Absorption spectra were recorded at room temperature using a PerkinElmer Lambda 35 UV/Vis spectrometer. Uncorrected

steady-state emission and excitation spectra were recorded using an Edinburgh FLSP980-stm spectrometer equipped with a 450 W xenon arc lamp, double excitation and emission monochromators, a Peltier-cooled Hamamatsu R928P photomultiplier (185–850 nm) and a Hamamatsu R5509-42 photomultiplier for detection of NIR radiation (800–1400 nm). Emission and excitation spectra were corrected for source intensity (lamp and grating) and emission spectral response (detector and grating) by a calibration curve supplied with the instrument. Overall quantum yields (Φ^{L}_{Ln}) were measured with the use of an integrating sphere coated with BenFlect.[36] In the case of the NIR, overall quantum yields were measured using two different detectors and [Yb(phen)(tta)$_3$] in toluene (Φ^{L}_{Ln} = 1.6%),[37] where tta is thenoyltrifluoroacetone, as reference to calibrate the set up according to the procedure previously reported by our group.[9]

Excited-state decays (τ) were recorded on the same Edinburgh FLSP980-stm spectrometer using a microsecond flashlamp. The goodness of fit was assessed by minimising the reduced χ^2 function and by visual inspection of the weighted residuals.

Synthesis

Di(4-methylbenzoyl)methane (mdbmH). The **mdbm**H precursor was synthesised following a previously reported procedure.[20]

Lanthanoid assemblies. RbOH (21 mg, 0.02 mmol) was added to a mixture containing **mtbm**H (74 mg, 0.20 mmol) and hydrated $LnCl_3$ (18 mg, 0.05 mmol) in ethanol (10 mL). The mixture was heated at reflux for 30 minutes and filtered over a glass frit while still hot. The filtered solution was then left undisturbed at ambient temperature and slow evaporation of the solvent over several days afforded crystals suitable for X-ray diffraction.

*{[Eu(Rb)(**mtbm**)$_4$]$_2$}$_n$.* 36 mg, 21%. M.p. 267–269 °C. Elemental analysis calcd (%) for $C_{200}H_{168}Rb_2Eu_2O_{24}$ (1.75·H_2O): C, 68.53; H, 5.05; found: C, 68.53; H, 4.74. IR (ATR): ν = 2919 w, 1634 w, 1602 m, 1577 m, 1538 s, 1408 m, 1360 s, 1275 m, 1183 m, 1151 m, 1115 w, 1021 w, 899 s, 837 m, 7836 s, 721 m, 694 w.

*{[Nd(Rb)(**mtbm**)$_4$]$_2$}$_n$.* 28 mg, 16%. M.p. 289–291 °C. Elemental analysis calcd (%) for $C_{100}H_{84}RbNdO_{12}$ (1.5·H_2O): C, 66.49; H, 5.30; found: C, 66.24; H, 4.93. IR (ATR): ν = 2920 w, 2164 w, 1634 m, 1602 m, 1574 m, 1529 s, 1405 m, 1342 s, 1273 m, 1184 m, 1151 m, 1112 w, 1034 w, 899 s, 825 m, 780 s, 763 s, 721 m.

*[Nd(Rb·HOEt)(**tbm**)$_4$]$_2$.* 21 mg, 13%. M.p. 259–261 °C. Elemental analysis calcd (%) for $C_{180}H_{132}Rb_2Nd_2O_{26}$: C, 68.19; H, 4.20; found: C, 67.70; H, 3.78. IR (ATR): ν = 3065 w, 1739 w, 1644 w, 1645 w, 1597 w, 1583 m, 1540 m, 1491 w, 1448 m, 1374 s, 1297 s, 1277 s, 1181 w, 1151 m, 1073 w, 1012 w, 897 s, 823 m, 779 w, 747 s.

Crystallography

Crystallographic data for the structures were collected at 100(2) K on an Oxford Diffraction Gemini or Xcalibur diffractometer using Mo Kα or Cu Kα radiation. Following absorption corrections and solution by direct methods, the structures were refined against F^2 with full-matrix least-squares using the SHELX-2014 crystallographic package.[38]

Unless stated below, anisotropic displacement parameters were employed for the non-hydrogen atoms. All hydrogen atoms were added at calculated positions and refined by use of a riding model with isotropic displacement parameters based on those of the parent atom.

{[Eu(Rb)(mtbm)$_4$]$_2$}$_n$. $C_{200}H_{168}Eu_2O_{24}Rb_2$·($H_2O$), M = 3448.20, crystal size 0.23 × 0.07 × 0.05 mm^3, triclinic, space group $P\bar{1}$ (No. 2), a = 14.9383(5), b = 15.9699(4), c = 17.9990(7) Å, α = 84.625(2), β = 74.799(3), γ = 88.086(2)°, V = 4125.3(2) Å^3, Z = 1, D_c = 1.388 g cm^{-3}, μ = 6.673 mm^{-1}. F_{000} = 1770, Cu Kα radiation, λ = 1.54178 Å, $2\theta_{max}$ = 134.8°, 44 958 reflections collected, 14 682unique (R_{int} = 0.0549). Final GooF = 1.059, R_1 = 0.0386, wR_2 = 0.0890, R indices based on 13 164 reflections with $I > 2\sigma(I)$, $|\Delta\rho|_{max}$ = 0.67 e Å^{-3}, 1054 parameters, 3 restraints. The water molecule hydrogen atoms were refined with geometries restrained to ideal values. CCDC 1829212.†

{[Nd(Rb)(mtbm)$_4$]$_2$}$_n$. $C_{200}H_{168}Nd_2O_{24}Rb_2$·($H_2O$), M = 3432.77, crystal size 0.167 × 0.044 × 0.028 mm^3, triclinic, space group $P\bar{1}$ (no. 2), a = 14.9907(3), b = 15.9632(3), c = 17.9930(4) Å, α = 84.954(2), β = 74.674(2), γ = 88.124(2)°, V = 4136.30(15) Å^3, Z = 1, D_c = 1.378 g cm^{-3}, μ = 6.017 mm^{-1}. F_{000} = 1764, Cu Kα radiation, λ = 1.54178 Å, $2\theta_{max}$ = 134.6°, 89 010 reflections collected, 14 738unique (R_{int} = 0.0665). Final GooF = 1.001, R_1 = 0.0335, wR_2 = 0.0787, R indices based on 13 047 reflections with $I > 2\sigma(I)$, $|\Delta\rho|_{max}$ = 0.84 e Å^{-3}, 1054 parameters, 9 restraints. The water molecule hydrogen atoms were refined with geometries restrained to ideal values. CCDC 1829213.†

[Nd(Rb·HOEt)(tbm)$_4$]$_2$. $C_{180}H_{132}Nd_2O_{26}Rb_2$·2($C_2H_6O$), M = 3262.40, crystal size 0.31 × 0.21 × 0.12 mm^3, triclinic, space group $P\bar{1}$ (no. 2), a = 14.0539(2), b = 14.7835(3), c = 19.7708(4) Å, α = 99.829(2), β = 107.431(2), γ = 90.137(2)°, V = 3855.27(13) Å^3, Z = 1, D_c = 1.405 g cm^{-3}, μ = 1.367 mm^{-1}. F_{000} = 1666, Mo Kα radiation, λ = 0.71073 Å, $2\theta_{max}$ = 64.7°, 84 599 reflections collected, 25 545unique (R_{int} = 0.0650). Final GooF = 1.002, R_1 = 0.0496, wR_2 = 0.0959, R indices based on 19 518 reflections with $I > 2\sigma$ (I), $|\Delta\rho|_{max}$ = 1.1 e Å^{-3}, 961 parameters, 13 restraints. One phenyl ring and two solvent ethanol molecules were modelled as being disordered over two sets of sites with occupancies constrained to 0.5 and with the non-hydrogen atoms refined with isotropic displacement parameters. Geometries of the disordered atoms were restrained to ideal values. CCDC 1829214.†

[Yb(mtbm)$_3$(OH$_2$)]$_2$. $C_{75}H_{65}O_{10}Yb$·0.5(C_2H_6O), M = 1322.34, crystal size 0.31 × 0.042 × 0.038 mm^3, monoclinic, space group $P2_1/n$, a = 10.5065(12), b = 22.8219(3), c = 26.2567(3) Å, β = 90.116(2)°, V = 6295.8(7) Å^3, Z = 4, D_c = 1.395 g cm^{-3}, μ = 3.245 mm^{-1}. F_{000} = 2712, Cu Kα radiation, λ = 1.54178 Å, $2\theta_{max}$ = 134.9°, 66 086 reflections collected, 11 254unique (R_{int} = 0.0839). Final GooF = 1.069, R_1 = 0.0486, wR_2 = 0.1117, R indices based on 8726 reflections with $I > 2\sigma(I)$, $|\Delta\rho|_{max}$ = 1.7 e Å^{-3}, 820 parameters, 17 restraints. The solvent was modelled as an ethanol molecule disordered about a crystallographic inversion centre. Geometries were restrained to ideal values.

Water molecule hydrogen atoms were located and refined with geometries restrained to ideal values. CCDC 1829215.†

[Nd(Cs·2HOEt)(dbm)$_4$]$_n$. $C_{64}H_{56}CsNdO_{10}$, M = 1262.23, crystal size 0.26 × 0.084 × 0.053 mm^3, monoclinic, space group $C2/c$, a = 27.4726(6), b = 8.29060(10), c = 25.4388(6) Å, β = 108.315(2)°, V = 5500.5(2) Å^3, Z = 4, D_c = 1.524 g cm^{-3}, μ = 12.772 mm^{-1}. F_{000} = 2540, Cu Kα radiation, λ = 1.54178 Å, $2\theta_{max}$ = 134.6°, 29 516 reflections collected, 4906 unique (R_{int} = 0.0436). Final GooF = 1.090, R_1 = 0.0386, wR_2 = 0.1095, R indices based on 4314 reflections with $I > 2\sigma(I)$, $|\Delta\rho|_{max}$ = 2.5 e Å^{-3}, 349 parameters, 0 restraints. CCDC 1829216.†

[Cs(mtbm)]$_n$. $C_{25}H_{21}CsO_3$, M = 502.33, crystal size 0.240 × 0.057 × 0.042 mm^3, monoclinic, space group $P2_1/c$, a = 8.41028 (14), b = 31.2556(4), c = 8.01519(14) Å, β = 102.777(2)°, V = 2054.77(6) Å^3, Z = 4, D_c = 1.624 g cm^{-3}, μ = 14.245 mm^{-1}. F_{000} = 1000, Cu Kα radiation, λ = 1.54178 Å, $2\theta_{max}$ = 134.6°, 17 616 reflections collected, 3671 unique (R_{int} = 0.0558). Final GooF = 1.037, R_1 = 0.0455, wR_2 = 0.1174, R indices based on 3361 reflections with $I > 2\sigma(I)$, $|\Delta\rho|_{max}$ = 2.4 e Å^{-3}, 265 parameters, 0 restraints. CCDC 1829217.†

Results and discussion

The **tbm**H and **mtbm**H molecules were synthesised according to the previously reported methodology.[20,39] Following a similar procedure to that previously reported for the preparation of {[Ln(Cs)(**tbm**)$_4$]$_2$}$_n$ (Ln^{3+} = Eu, Er, Yb) and {[Ln(Cs)(**mtbm**)$_4$]$_2$}$_n$ (Ln^{3+} = Eu, Er),[20] one equivalent of hydrated $LnCl_3$ (Ln^{3+} = Eu, Nd) was made to react with four equivalents of **mtbm**H and four equivalents of RbOH in ethanol. Slow evaporation of the solvent resulted in the formation of suitable crystals for X-ray diffraction, revealing the formation of coordination polymers with formula {[Ln(Rb)(**mtbm**)$_4$]$_2$}$_n$ where Ln^{3+} = Eu(**1**), Nd(**2**). The compositions of the isolated species were further confirmed by elemental analysis and IR spectroscopy. The resulting solids are isolated with variable degrees of solvation, which has been found previously for these Ln^{3+}/Ae$^+$ based complexes.[19,20]

The Eu^{3+}/Nd^{3+} mixed assemblies were synthesised in a similar fashion to the {[Ln(Rb)(**mtbm**)$_4$]$_2$}$_n$, except for the use of mixtures of hydrated $EuCl_3$ and $NdCl_3$ in molar ratios of Nd^{3+} of 0.25 (**3**), 0.50 (**4**) and 0.75 (**5**).

Analogous syntheses were attempted with CsOH and $NdCl_3$ in order to assess the effect of the different alkaline base in the mixed systems. However, only the cesium-containing coordination polymer [Cs(**mtbm**)]$_n$ was deposited (ESI†).[20]

When the same procedure was followed for the hydrated $NdCl_3$ and **tbm**H with RbOH or CsOH, the formation of assemblies with formula [Nd(Rb)(**tbm**)$_4$]$_2$ and [Nd(Cs·2HOEt)(**dbm**)$_4$]$_n$ was found, respectively. The [Nd(Rb)(**tbm**)$_4$]$_2$ (**6**) complex presents a similar structure to the previously reported tetranuclear assemblies.[19] In contrast, the isolation of the [Nd(Cs·2HOEt)(**dbm**)$_4$]$_n$ linear polymer shows the second example of a possible *in situ* retro-Claisen condensation reaction of **tbm**H in the presence of CsOH and hydrated $NdCl_3$ resulting in the formation of a β-diketonate complex similar to previously reported examples (ESI†).[20] The hypothesis that the triketonate ligands undergo a retro-Claisen condensation reaction under these reaction conditions is currently under investigation and the results will be presented elsewhere.

Finally, when the same procedure was attempted with $YbCl_3$, a dimeric structure was crystallised with formula [Yb(**mtbm**)$_3$(H$_2$O)$_2$]$_2$ (ESI†). Due to difference in composition and symmetry of this structure in comparison with the polymeric species of complexes **1** and **2**, Yb^{3+} was not further investigated for the purpose of this study.

Crystal structures

The structures of the two {[Ln(Rb)(**mtbm**)$_4$]$_2$}$_n$ (Ln^{3+} = Nd, Eu) complexes are isomorphous and structurally similar to the previously reported Cs-based polymers with formula {[Ln(Cs)(mtbm)$_4$]$_2$}$_n$ (Ln^{3+} = Eu, Er).[20] See Table 1 for a list of bond lengths and angles. The units formed of two Ln^{3+}, two Rb$^+$ metal centres and eight **mtbm**$^-$ ligands are isomorphous to the previously reported tetranuclear assemblies.[18] The Ln^{3+} is eight coordinated, with four **mtbm**$^-$ ligands coordinated by two of the *O*-keto atoms in a bidentate mode. In this case, the third *O*-keto of two of the ligands are linked to Rb$^+$ cations forming the tetranuclear assembly and the polymer, respectively (Fig. 1).

Here, a H_2O molecule is found in the lattice with two hydrogen bonds formed with two keto O(22) and O(31).

Table 1 Selected bond lengths and intermetallic distances (Å) for complexes **1**, **2** and **6**

	1 {[**Eu**(Rb)(mtbm)$_4$]$_2$}$_n$	**2** [**Nd**(Rb)(mtbm)$_4$]$_2$}$_n$	**6** [**Nd**(Rb·HOEt)(tbm)$_4$]$_2$
Ln–O	2.327(2)–2.405(2)	2.363(2)–2.444(2)	2.390(2)–2.450(2)
Ae–O	2.816(2)–2.983(2)	2.817(2)–2.989(2)	2.822(2)–3.051(2)
Ae(1)–Ae(2)	8.1196(5)	8.1312(5)	8.3053(6)
Ae(1)–Ae(2^a)	8.7992(5)	8.8013(5)	–
Ln(1)–Ln(2)	9.4915(5)	9.5391(5)	8.9836(5)
Ln(1)–Ln(2^a)	11.0901(6)	11.0929(5)	13.8915(6)
Ln(1)–Ae(1)	4.0943(4)	4.1044(3)	4.1340(3)
Ln(1)–Ae(2)	8.1849(5)	8.8169(5)	7.5993(6)
Ae(2)–Ln(1^a)	8.8145(5)	8.2087(5)	—
Ln(1)–Ln(1^b)	14.9383(7)	14.9907(5)	14.0539(5)

^{a} Subsequent units. ^{b} Different chain.

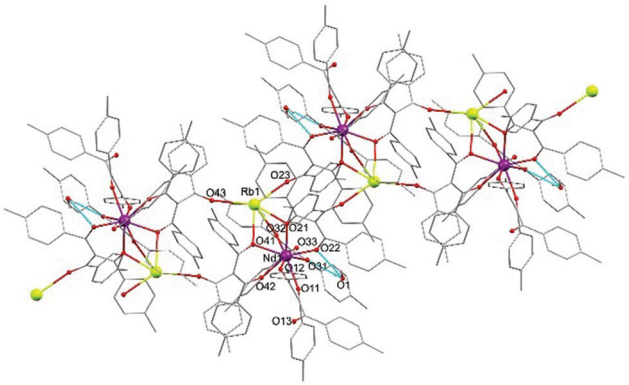

Fig. 1 Representation of the X-ray structure of **2**, $\{[Nd(Rb)(\mathbf{mtbm})_4]_2\}_n$, where hydrogen atoms have been omitted for clarity.

Intermolecular interactions between chains are present where the lanthanoid centres sit at distances longer than 14 Å (ESI†). The geometry of the eight coordinate Ln^{3+} is best described as triangular dodecahedron (ESI†).

The structure of the $[Nd(Rb{\cdot}HOEt)(\mathbf{tbm})_4]_2$ is isomorphous to the previously published tetranuclear assemblies with

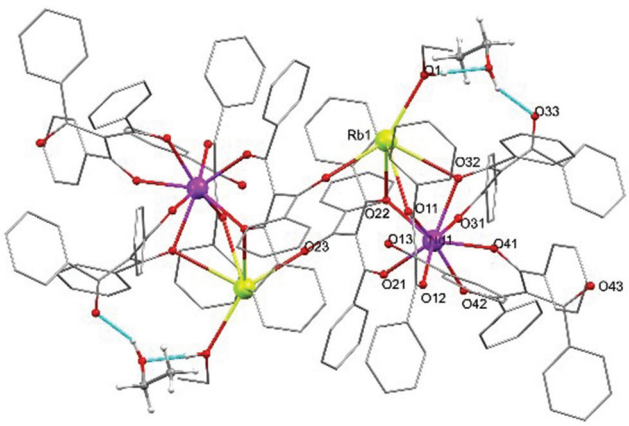

Fig. 2 Representation of the X-ray structure of **6**, $[Nd(Rb)(\mathbf{tbm})_4]_2$, where hydrogen atoms have been omitted for clarity except for those on the solvent EtOH molecule.

Ln^{3+} = Eu^{3+}, Er^{3+} and Yb^{3+}.[19] where the eight coordinated Nd^{3+} adopts a geometry best described as distorted triangular dodecahedron (Fig. 2).

Photophysical investigation

The photophysical data for complexes **1–6** including excited state lifetime decay (τ_{obs}), calculated radiative decay (τ_R), intrinsic photoluminescence quantum yield (Φ_{Ln}^{Ln}), overall photoluminescence quantum yield (Φ_{Ln}^{Ln}) and calculated sensitisation efficiency (η_{sens}), are reported in Table 2. The emission properties were recorded in the solid state due to the low stability of the complexes in polar solvents and poor solubility in nonpolar solvents, as previously demonstrated for analogous systems.[18]

As shown before, the energy of the **mtbm** and **tbm** triplet states (21 140 cm^{-1} and 20 704 cm^{-1})[18,20] are sufficiently high to sensitise the $^5D_0$ (~17 200 cm^{-1}) of Eu^3, the $^2F_{5/2}$ (~10 200 cm^{-1}) of Yb^{3+} and the $^4I_{13/2}$ (~6566 cm^{-1}) of Er^{3+}. Therefore, energy transfer to the $^4F_{3/2}$ (~11 260 cm^{-1}) state of Nd^{3+} is also expected. In fact, each emission spectrum shown herein is the result of an effective antenna effect, a conclusion that is supported by the broad excitation spectra which match with the absorption profile of the corresponding ligands.

The emission spectrum of $\{[Eu(Rb)(\mathbf{mtbm})_4]_2\}_n$ (**1**) shows the characteristic Eu^{3+} emission bands attributed to the $^7F_J \leftarrow {}^5D_0$ (J = 0–6) region 580–820 nm (Fig. 3).[40,41] The $^7F_0 \leftarrow {}^5D_0$ transition is strictly forbidden by the selection rules and is only observable for low symmetry complexes. The magnetic dipole-allowed band ($^7F_1 \leftarrow {}^5D_0$) is split into two sublevels inherent to tetragonal crystal fields. This is in agreement with the splitting of the hypersensitive band ($^7F_2 \leftarrow {}^5D_0$) in four sublevels. The splitting of the main transitions is in accordance with the shape analysis, which suggests that the local symmetry of the Eu^{3+} cation is best described as a distorted triangular dodecahedron.

The excited state decay was satisfactorily fitted as a monoexponential function, giving a value of observable lifetime (τ_{obs}) of 507 μs. From the emission spectrum, the radiative decay (τ_r) was calculated to be 0.86 ms. With an integrating sphere, the overall quantum yield (Φ_{Ln}^{L}) was measured as 31%. From these

Table 2 Photophysical data for the complexes in the solid state

Complex	$\chi_{Nd^{3+}}$ [a]	λ_{em} [b] (nm)	τ_{obs} (μs)	τ_r (ms)	$\Phi^{Ln}{}_{Ln}$ (%)	$\Phi^{L}{}_{Ln}$ [c] (%)	η_{sens}	k_{ET} (s^{-1})	τ_{ET} (s)	Φ_{ET} (%)
1 $\{[Eu(Rb)(\mathbf{mtbm})_4]_2\}_n$	0	612 (Eu^{3+})	507	0.86	59	31	52	—	—	—
2 $\{[Nd(Rb)(\mathbf{mtbm})_4]_2\}_n$	1	1060 (Nd^{3+})	11	0.27[d]	4.2	1.34	32	—	—	—
3 $\{[Eu_{1-x}Nd_x(Rb)(\mathbf{mtbm})_4]_2\}_n$	0.25	612(Eu^{3+})	335	0.681	49	17.5	35	1.0×10^3	9.87×10^{-4}	34
		1060 (Nd^{3+})	8.7	0.27[d]	3.1	0.23	7			
4 $\{[Eu_{1-x}Nd_x(Rb)(\mathbf{mtbm})_4]_2\}_n$	0.5	612(Eu^{3+})	183	0.46	40	6.55	16	3.5×10^3	2.86×10^{-4}	64
		1060 (Nd^{3+})	11.0	0.27[d]	4.1	0.74	18			
5 $\{[Eu_{1-x}Nd_x(Rb)(\mathbf{mtbm})_4]_2\}_n$	0.75	612(Eu^{3+})	143	0.54	27	1.44	5	5.0×10^3	1.99×10^{-4}	72
		1060 (Nd^{3+})	8.7	0.27[c]	3.2	0.44	14			
6 $[Nd(Rb{\cdot}HOEt)(\mathbf{tbm})_4]_2$	1	1060 (Nd^{3+})	8.8	0.27[d]	3.3	0.58	17	—	—	—

[a] Solution phase compositions in the reaction mixture. [b] Emission spectra recorded using λ_{exc} = 350 nm. [c] Quantum yield measured with the use of an integrating sphere. [d] Literature value for Nd^{3+}.[16]

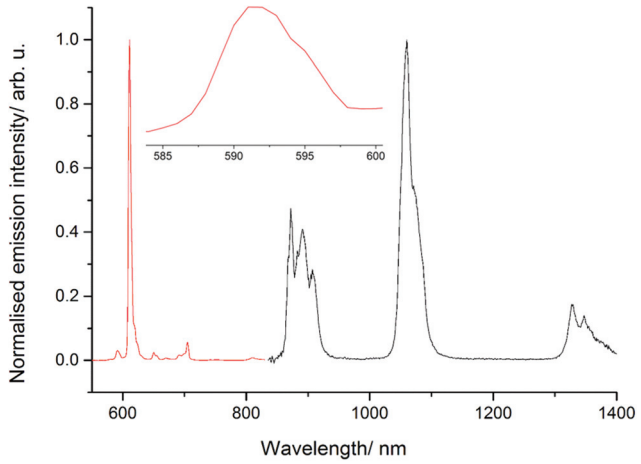

Fig. 3 Normalised emission plot for $\{[Eu(Rb)(\mathbf{mtbm})_4]_2\}_n$ (red trace) and $\{[Nd(Rb)(\mathbf{mtbm})_4]_2\}_n$ (black trace) in the solid state, with excitation wavelength at 350 nm. Inset: highlight of the splitting of the magnetic dipole transition for the Eu^{3+} complex.

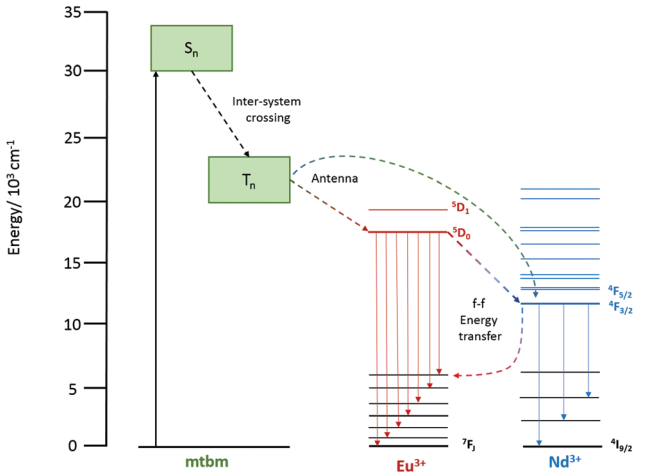

Fig. 4 Energy level diagram and energy transfer occurring for the mixed complexes $\{[Eu_{1-x}Nd_x(Rb)(\mathbf{mtbm})_4]_2\}_n$.

data, the intrinsic quantum yield (Φ_{Ln}^{Ln}) as ratio τ_{obs}/τ_r could be calculated to be 59% with a sensitisation efficiency of 52%.

These data are of the same order as the previously reported $\{[Eu(Cs)(\mathbf{mtbm})_4]_2\}_n$,[20] showing that the exchange in the alkaline base has little impact on the photophysical properties.

The emission spectrum of $\{[Nd(Rb)(\mathbf{mtbm})_4]_2\}_n$ (**2**) shows the characteristic Nd^{3+} emission bands from the $^4I_J \leftarrow {}^4F_{3/2}$ (J = 9/2, 11/2, 13/2) with maxima at 910, 1060 and 1350 nm respectively (Fig. 3).[42] These bands are structured as a consequence of the crystal field effect from the ligands. The excited state decay was measured to be 11 μs after deconvolution from instrumental response. This value of τ_{obs} is relatively high in comparison to the previously reported β-diketonate compounds[21,28] and of the same order of magnitude as highly conjugated systems where the triplet state is lowered in energy to better match the emissive lanthanoid excited state energy.[14,43]

Although it is known that the radiative decay for Nd^{3+} ranges from 0.2 to 0.5 ms,[4] a standard value of 0.27 ms is generally accepted for the Nd^{3+} complexes in the solid state.[16] The intrinsic quantum yield can therefore be estimated to 4.2%. The overall quantum yield, using an integrating sphere following previously reported procedure for the use of two different detectors,[9] was found to be 1.34%, with a sensitisation efficiency of 32%. These data highlight that reducing non-radiative decays due to the removal of the C–H bond is an effective way to enhance the photophysical properties of the Nd^{3+} emitters.

As the structures for Eu^{3+} and Nd^{3+} are isomorphous, $\{[Ln(Rb)(\mathbf{mtbm})_4]_2\}_n$, mixtures of both lanthanoids were prepared (**3**–**5**) in order to investigate sensitisation of the $^4F_{3/2}$ of Nd^{3+} *via* the $^5D_0$ of Eu^{3+} (Fig. 4).

The emission spectra of the mixed complexes show the characteristic emission bands from the $^7F_J \leftarrow {}^5D_0$ (J = 0–6) of Eu^{3+} in the visible region (580–820 nm) and the $^4I_J \leftarrow {}^4F_{3/2}$ (J = 9/2, 11/2, 13/2) Nd^{3+} bands in the NIR region (850–1400 nm) with identical splitting in comparison with the pure complexes **1** and **2**, respectively. This suggests that the structure is preserved with the mixed lanthanoid polymers. The intensity of the Nd^{3+} emission bands increases when the molar ratio of Nd^{3+} is higher (Fig. 5). The lifetime of the excited state of Eu^{3+} is shortened as the amount of Nd^{3+} increases, from 507 μs for **1** (where Nd^{3+} is absent) to 335 μs, 183 μs and 143 μs for **3**, **4** and **5**, respectively. From these numbers, the highest energy transfer quantum efficiency can be calculated to be 72% for complex **5**. Overall quantum yields were measured, finding decreasing values for Eu^{3+} of 17.5%, 6.55% and 1.44% for complexes **3**–**5**, respectively (Table 2). In the case of Nd^{3+}, both lifetime and overall quantum yield values seem to be reduced by the presence of Eu^{3+}. These results indicate possible quenching of the $^4F_{3/2}$ of Nd^{3+} by the ^7F_J of Eu^{3+} as previously suggested in the literature.[34] However, the ratio of this energy transfer was calculated to be only 20%, which is perhaps the

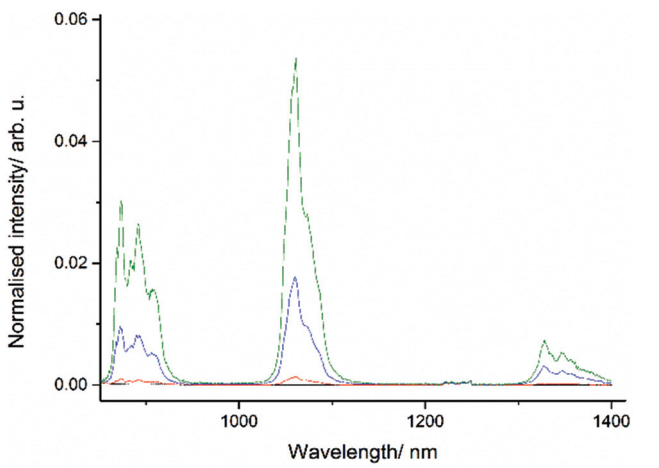

Fig. 5 Nd^{3+} emission plot for complex **2** (black trace), **3** (red trace), **4** (blue trace) and **5** (green trace) with excitation wavelength at 350 nm normalised at 612 nm (Eu^{3+} emission).

main difference from previous Eu/Nd coordination compounds where no neodymium emission was reported.[30–32]

Typically, energy transfer between lanthanoid centres is considered limited for distances longer than 9 Å because of slow energy migration.[44] In fact, if a purely dipole–dipole exchange mechanism is considered, the donor–acceptor distance can be calculated to be 7.7 Å following eqn (6), for a quantum efficiency of energy transfer (Φ_{ET}) of 0.72 for complex **5**. However, in our system and when considering one polymeric chain, the shortest distance between two lanthanoid centres is 9.5 Å. Therefore, the sensitisation to *f states of Nd^{3+} from the $^5D_0$ of Eu^{3+} for complexes **3–5** seems not to be a pure Förster mechanism, and a ligand-mediated Dexter mechanism may have some contribution.[45,46]

As a control experiment, equimolar mechanically-ground mixtures of **1** and **2** were studied. The lifetime of the $^5D_0$ of Eu^{3+} was found to be 356 μs, shorter than the pure complex **1** (τ_{obs} = 507 μs) and longer with respect to the solution-phase mixed equimolar complex **4** (τ_{obs} = 507 μs). These data suggest that there is energy transfer between chains occurring at 30% of efficiency. Taking into consideration the long Ln–Ln distances between chains (~15 Å) based on the crystal structure, the energy transfer process may occur *via* intermolecular interactions (ESI†).

Finally, the emission spectrum of $[Nd(Rb{\cdot}HOEt)(\mathbf{tbm})_4]_2$ (**6**) shows the three characteristic Nd^{3+} bands from the $^4I_J \leftarrow {}^4F_{3/2}$ (J = 9/2, 11/2, 13/2) similarly to the $\{[Nd(Rb)(\mathbf{mtbm})_4]_2\}_n$ (**1**) (ESI†). The values of lifetime (τ_{obs}), intrinsic quantum yield (Φ_{Ln}^{Ln}) and overall quantum yield (Φ_{Ln}^{L}) were found to be 8.85 μs, 3.3% and 0.58%, respectively. The main difference with complex **2** arises from a lower overall quantum yield, maintaining the values of lifetime and intrinsic quantum yields, which suggests that the sensitisation process from **tbm** to the 4f* accepting states of Nd^{3+} is not as efficient as in the **mtbm** based complexes.

Conclusions

In this report the study of β-triketonate based lanthanoid complexes has been extended to Nd^{3+}, presenting new examples of tetranuclear assemblies ($[Nd(Rb{\cdot}HOEt)(\mathbf{tbm})_4]_2$) and coordination polymers with formula $\{[Nd(Rb)(\mathbf{mtbm})_4]_2\}_n$. The fact that isomorphous structures were found for the **mtbm** and Eu^{3+} ($\{[Nd(Rb)(\mathbf{mtbm})_4]_2\}_n$), opened up the possibility to synthesise mixed lanthanoid complexes with the aim of achieving f–f energy transfer. Indeed, an example of a mixed **mtbm** based lanthanoid coordination polymer with efficient sensitisation from the $^5D_0$ of Eu^{3+} to the $^4F_{3/2}$ of Nd^{3+} was formulated. The emission studies of the pure and mixed complexes show particularly good photophysical properties in the case of Nd^{3+} *via* both mechanisms: standard antenna and f–f sensitisation.

Conflicts of interest

There are no conflicts to declare.

Acknowledgements

This research was partially supported by the Australian Research Council's Discovery *Projects* funding scheme (project DP170101895), and a Royal Society International Exchanges Grant. E. Z.-C. thanks the EPSRC (EP/M02105X/1) for support. L. A. G thanks Curtin University for the Australian Postgraduate Award. The authors acknowledge access to the facilities at the Centre for Microscopy, Characterisation and Analysis, University of Western Australia.

Notes and references

1 S. V. Eliseeva and J.-C. G. Bünzli, *Chem. Soc. Rev.*, 2010, **39**, 189–227.
2 J.-C. G. Bünzli, *Luminescence Bioimaging with Lanthanide Complexes*, 2014, vol. 1st.
3 J.-C. G. Bünzli and S. V. Eliseeva, *J. Rare Earths*, 2010, **28**, 824–842.
4 J.-C. G. Bünzli and S. V. Eliseeva, *Photophysics of Lanthanoid Coordination Compounds*, 2013, vol. 8.
5 V. V. Utochnikova, A. Grishko, A. Vashchenko, A. Goloveshkin, A. Averin and N. Kuzmina, *Eur. J. Inorg. Chem.*, 2017, 1–6.
6 S. V. Eliseeva and J.-C. G. Bünzli, *New J. Chem.*, 2011, **35**, 1165.
7 J.-C. G. Bünzli and S. V. Eliseeva, *Springer Ser. Fluoresc.*, 2011, 1–45.
8 S. Cotton, *Lanthanide and Actinide Chemistry*, 2005.
9 L. Abad Galán, B. L. Reid, S. Stagni, A. N. Sobolev, B. W. Skelton, E. G. Moore, G. S. Hanan, E. Zysman-Colman, M. I. Ogden and M. Massi, *Dalton Trans.*, 2018, **47**, 7956–7964.
10 O. Sun, T. Gao, J. Sun, G. Li, H. Li, H. Xu, C. Wang and P. Yan, *CrystEngComm*, 2014, **16**, 10460–10468.
11 N. M. Shavaleev, S. J. A. Pope, Z. R. Bell and M. D. Ward, *Dalton Trans.*, 2003, **0**, 808–814.
12 G. Zucchi, O. Maury, P. Thuéry and M. Ephritikhine, *Inorg. Chem.*, 2008, **47**, 10398–10406.
13 W. Li, J. Li, H. Li, P. Yan, G. Hou and G. Li, *J. Lumin.*, 2014, **146**, 205–210.
14 L. Yang, Z. Gong, D. Nie, B. Lou, Z. Bian, M. Guan, C. Huang, H. J. Lee and W. P. Baik, *New J. Chem.*, 2006, **30**, 791.
15 M. Iwamuro, Y. Wada, T. Kitamura and N. Nakashima, *Phys. Chem. Chem. Phys.*, 2000, **2**, 2291–2296.
16 T. M. George, S. Varughese and M. L. P. Reddy, *RSC Adv.*, 2016, **6**, 69509–69520.
17 B. Li, H. Li, P. Chen, W. Sun, C. Wang, T. Gao and P. Yan, *Dalton Trans.*, 2016, **45**, 11459–11470.
18 B. L. Reid, S. Stagni, J. M. Malicka, M. Cocchi, G. S. Hanan, M. I. Ogden and M. Massi, *Chem. Commun.*, 2014, **50**, 11580–11582.
19 B. L. Reid, S. Stagni, J. M. Malicka, M. Cocchi, A. N. Sobolev, B. W. Skelton, E. G. Moore, G. S. Hanan,

M. I. Ogden and M. Massi, *Chem. – Eur. J.*, 2015, **21**, 18354–18363.
20 L. Abad Galán, B. L. Reid, S. Stagni, A. N. Sobolev, B. W. Skelton, M. Cocchi, J. M. Malicka, E. Zysman-colman, E. G. Moore, M. I. Ogden and M. Massi, *Inorg. Chem.*, 2017, **56**, 8975–8985.
21 X. Rao, T. Song, J. Gao, Y. Cui, Y. Yang, C. Wu, B. Chen and G. Qian, *J. Am. Chem. Soc.*, 2013, **135**, 15559–15564.
22 D. T. De Lill, A. De Bettencourt-Dias and C. L. Cahill, *Inorg. Chem.*, 2007, **46**, 3960–3965.
23 S. Freslon, Y. Luo, G. Calvez, C. Daiguebonne, O. Guillou, K. Bernot, V. Michel and X. Fan, *Inorg. Chem.*, 2014, **53**, 1217–1228.
24 F. Artizzu, A. Serpe, L. Marchiò, M. Saba, A. Mura, M. L. Mercuri, G. Bongiovanni, P. Deplano and F. Quochi, *J. Mater. Chem. C*, 2015, **3**, 11524–11530.
25 L. Song, Q. Wang, D. Tang, X. Liu and Z. Zhen, *New J. Chem.*, 2007, **31**, 506–511.
26 S. Hinojosa, M. A. Meneses-Nava, O. Barbosa-García, L. A. Díaz-Torres, M. A. Santoyo and J. F. Mosiño, *J. Lumin.*, 2003, **102–103**, 694–698.
27 F. Artizzu, F. Quochi, L. Marchiò, E. Sessini, M. Saba, A. Serpe, A. Mura, M. L. Mercuri, G. Bongiovanni and P. Deplano, *J. Phys. Chem. Lett.*, 2013, **4**, 3062–3066.
28 S. Faulkner and S. J. A. Pope, *J. Am. Chem. Soc.*, 2003, **125**, 10526–10527.
29 L. Zhou, P. A. Tanner, W. Zhou, Y. Ai, L. Ning, M. M. Wu and H. Liang, *Angew. Chem., Int. Ed.*, 2017, **56**, 10357–10361.
30 J.-C. G. Bünzli and F. Ihringer, *Inorg. Chim. Acta*, 1996, **246**, 195–205.
31 C. M. Andolina and J. R. Morrow, *Eur. J. Inorg. Chem.*, 2010, **2011**, 154–164.
32 J. J. Lessmann and W. D. W. Horrocks, *Inorg. Chem.*, 2000, **39**, 3114–3124.
33 L. G. Van Uitert, E. F. Dearborn and J. J. Rubin, *J. Chem. Phys.*, 1967, **46**, 3551–3555.
34 E. J. Sharp, M. J. Weber and G. Cleek, *J. Appl. Phys.*, 1970, **41**, 364–369.
35 W. D. W. Horrocks, M. J. Rhee, A. Peter Snyder and D. R. Sudnick, *J. Am. Chem. Soc.*, 1980, **102**, 3650–3652.
36 J. C. De Mello, H. F. Wittmann and R. H. Friend, *Adv. Mater.*, 1997, **9**, 230–232.
37 M. P. Tsvirko, S. B. Meshkova, V. Y. Venchikov, Z. M. Topilova and D. V. Bol'shoi, *Opt. Spectrosc.*, 2001, **90**, 669–673.
38 G. M. Sheldrick, *Acta Crystallogr. Sect. C Struct. Chem.*, 2015, **71**, 3–8.
39 B. L. Reid, S. Stagni, J. M. Malicka, M. Cocchi, G. S. Hanan, M. I. Ogden and M. Massi, *Chem. Commun.*, 2014, **50**, 11580–11582.
40 A. M. Hilder, P. C. Junk, U. H. Kynast and M. M. Lezhnina, *J. Photochem. Photobiol. A Chem.*, 2008, **202**, 10–20.
41 M. Hilder, M. Lezhnina, M. L. Cole, C. M. Forsyth, P. C. Junk and U. H. Kynast, *J. Photochem. Photobiol. A Chem.*, 2011, **217**, 76–86.
42 L. Hu, J. Zhang, Q. Yin, P. Li and K. Du, *Opt. Commun.*, 2014, **324**, 26–29.
43 S. I. Klink, G. A. Hebbink, L. Grave, P. G. B. Oude Alink, F. C. J. M. van Veggel and M. H. V. Werts, *J. Phys. Chem. A*, 2002, **106**, 3681–3689.
44 S. Omagari, T. Nakanishi, Y. Hirai, Y. Kitagawa, T. Seki, K. Fushimi, H. Ito and Y. Hasegawa, *Eur. J. Inorg. Chem.*, 2017, 1–8.
45 A. Zam, S. V. Eliseeva, L. Guønøe, H. Nozary, S. Petoud and C. Piguet, *Chem. – Eur. J.*, 2014, **20**, 12172–12182.
46 J.-C. G. Bünzli and C. Piguet, *Chem. Soc. Rev.*, 2005, **34**, 1048–1077.